Reaction Dynamics Study on the Tunneling Effects of a Microsolvated E2 Reaction: $FO^-(H_2O) + C_2H_5Cl \rightarrow HOF(H_2O) + C_2H_4 + Cl^-$

Yin-Ru Wu and Wei-Ping Hu*

Contribution from the Department of Chemistry, National Chung Cheng University, Chia-Yi, Taiwan 621

Received June 8, 1999. Revised Manuscript Received August 5, 1999

Abstract: Dual-level variational transition state theory with semiclassical tunneling (VTST/ST) calculation has been performed on the gas-phase microsolvated E2 reaction of $FO^-(H_2O) + C_2H_5Cl$. The high-level data are obtained using correlated extended-basis-set electronic structure calculations and the low-level potential energy surface is based on a PM3-SRP method. The classical barrier of the reaction is estimated to be 3−5 kcal/mol. The rate constants and the kinetic isotope effects (KIEs) were calculated from 200 to 800 K. Tunneling effects are found to contribute significantly to the rate constants at low temperatures in most cases. Interestingly, the tunneling effects contribute very inversely to the calculated KIEs at lower temperatures. The solvent kinetic isotope effects (SKIEs) are also calculated as a function of temperature at different barrier heights in the estimated barrier range. It is found that tunneling contributes normally to the inverse SKIEs. The results from the current study suggest that the tunneling effects in E2 reactions make both KIEs and SKIEs less pronounced at lower temperatures.

Introduction

A fundamental understanding of the ion−molecule S_N2 and E2 reactions, which usually involve an alkyl halide and a negative ion (the nucleophile), is very important since they are prototypes of substitution and elimination reactions that are ubiquitous in organic chemistry. Although the S_N2 reactions have attracted extensive theoretical investigation in recent years, there have been much fewer theoretical studies on the reaction dynamics of the E2 systems.These two types of ion−molecule reactions may be competitive with the same set of reactants, and they produce the same ionic product species. This makes it difficult to distinguish experimentally[3a] between these two reaction pathways. However, it has been known that the E2 reactions usually show strong normal kinetic isotope effects (KIEs) while the S_N2 reactions show a slightly inverse kinetic isotope effects.[3b,e,]The reasons for this difference have been studied previously[1a,b,5−8] with transition state theory (TST) and variational transition state theory (VTST)[9]for a few cases. It is found that the zero-point energy effects and the rotational partition functions are most responsible for the difference in the KIEs. For those reactions with very low barriers and at very low temperatures, the reaction bottleneck is dominated by the collision free energy barrier. In such cases, an interesting competition effect[1a] may result in dramatic KIEs. The dynamics behaviors of these ion−molecule reactions in the gas-phase have been studied less extensively for higher barrier cases. Due to the strong ion−dipole interaction, most S_N2 and E2 reactions in the gas phase have very low potential energy barriers in the exoergic direction. However, in the solution phase the transition states are less well solvated than the reactants and products, and thus the reactions may have significant central barriers. In such cases, especially for the E2 reaction, the tunneling effects may be important because the reaction involves a proton transfer from the alkyl halide to the negatively charged nucleophile. The tunneling effects not only may have a dramatic effect on the reaction rate constants but also can have significant contribution to the observed KIEs. To investigate these interesting effects quantitatively, we decided to perform a theoretical study on an E2 system with a significant barrier on *both* forward and reverse directions in order for tunneling to occur. Since there are not many gas-phase E2 systems that meet the above criterion, and accurate solution-phase dynamics study is not currently com-

* To whom correspondence should be addressed. E-mail: chewph@ccunix.ccu.edu.tw.

(1) Some of the most recent theoretical studies on gas-phase E2 reactions include: (a) Hu, W.-P.; Truhlar, D. G. *J. Am. Chem. Soc.* **1996**, *118*, 860. (b) Nielsen, P. A.; Glad, S. S.; Jensen F. *J. Am. Chem. Soc.* **1996**, *118*, 10577. (c) Merrill, G. N.; Gronert, S.; Kass, S. R. *J. Phys. Chem. A* **1997**, *101*, 208. (d) Chung D. S.; Kim, C. K.; Lee, B. S.; Lee, I. *J. Phys. Chem. A* **1997**, *101*, 9097. Many earlier representative theoretical and experimental studies on the E2 and S_N2 reactions can be found in the references of the above articles.

(2) Some of the most recent theoretical studies on gas-phase S_N2 reactions include: (a) Nakamura, E.; Mori, S.; Morokuma, K. *J. Am. Chem. Soc.* **1998**, *120*, 8273. (b) Mann, D. J.; Hase, W. L. *J. Phys. Chem. A,* **1998**, *102*, 6208. (c) Streitwieser, A.; Choy, G. S.-C.; Abu-Hasanayn, F. *J. Am. Chem. Soc.* **1997**, *119*, 5013. (d) Glukhovtsev, M. N.; Pross, A.; Schlegel H. B.; Bach, R. D.; Radom, L. *J. Am. Chem. Soc.*, **1996**, *118*, 11258. (e) Glukhovtsev, M. N.; Pross, A.; Radom, L. *J. Am. Chem. Soc.* **1996**, *118*, 6273.

(3) Some of the most recent experimental studies on E2 reactions include: (a) Flores, A. E.; Gronert S. *J. Am. Chem. Soc.* **1999**, *121*, 2627. (b) Cho, B. R.; Chung H. S.; Cho, N. S. *J. Org. Chem.* **1998**, *63*, 4685. (c) Cho, B. R, Kim, Y. K.; Yoon, C.-O. M. *J. Am. Chem. Soc.* **1997**, *119*, 691. (d) Meng, Q.; Gogoll, A.; Thibblin, A. *J. Am. Chem. Soc.* **1997**, *119*, 1217. (e) Meng, Q.; Thibblin, A. *J. Am. Chem. Soc.* **1997**, *119*, 1224.

(4) (a) de Koning, L. J.; Nibbering, N. M. M. *J. Am. Chem. Soc.* **1987**, *109*, 1715. (b) Gronert, S.; Depuy, C. H.; Bierbaum, V. M. *J. Am. Chem. Soc.* **1991**, *113*, 4009.

(5) Zhao, X. G.; Tucker, S. C.; Truhlar, D. G. *J. Am. Chem. Soc.* **1991**, *113*, 826.

(6) Poirier, R. A.; Wang, Y.; Westaway, K. C. *J. Am. Chem. Soc.* **1994**, *116*, 2526.

(7) Hu, W.-P.; Truhlar, D. G. *J. Am. Chem. Soc.* **1994**, *116*, 7797.

(8) Hu, W.-P.; Truhlar, D. G. *J. Am. Chem. Soc.* **1995**, *117*, 10726.

(9) Truhlar, D. G.; Garrett, B. C. *Acc. Chem. Res.* **1980**, *13*, 440.

10.1021/ja991901e CCC: $18.00
Published on Web 10/15/1999

putationally tractable, we turned our attention to systems between the gas- and solution phases. Recently, there have been considerable experimental[10] and theoretical[5,7,11] study on microsolvated ion−molecule systems in attempt to bridge the gap of our understanding between the gas-phase and solution-phase reactions. In the current study, we chose to investigate the dynamics behaviors, especially the tunneling effects, of a microsolvated E2 system of $OF^-(H_2O) + C_2H_5Cl \rightarrow HOF(H_2O) + C_2H_4 + Cl^-$. Of course, the S_N2 channel can compete with the E2 channel in this reaction. However, the current system serves primarily as a model system for those E2 reactions in which the tunneling and the solvent effects are important. Consequently, we will focus only on the E2 pathway in this study.

Methods

Electronic Structure Calculations. The geometry and energies of the reactants, products, the reactant-side complex, and the transition state were calculated at the Moller−Plesset sencond-order perturbation theory (MP2)[12] level with the following basis sets: (1) standard 6-31+G*,[13] (2) the ADZP basis sets, which, as discussed previously,[1a] consist of the cc-pVDZ[13] basis sets for carbon and hydrogen atoms, and aug-cc-pVDZ[13] basis sets without the *d* diffuse functions for oxygen, fluorine, and chlorine atoms, and (3) the full aug-cc-pVDZ basis sets. The vibrational frequencies of the stationary points were also calculated with the first two basis sets at the MP2 level. These calculations were carried out using Gaussian 94 program.[13] The stationary point properties were also calculated at the PM3[14] and the PM3-specific reaction parameter (PM3-SRP)[15] semiempirical levels. Two of PM3 parameters were modified in the PM3-SRP method to obtain better agreement in energies with the higher level electronic structure calculations and experiment. The PM3 method is chosen instead of another popular semiempirical method AM1[16] because we found that the AM1 method is unable to provide reasonable geometry and energy data for microsolvated systems. The semiempirical calculations were performed using the MOPAC 5.07mn program.[17]

The above calculations were carried out on an SGI Octane workstation in our research group and an SGI Origin 2000 server in the National Center for High Performance Computing in Taiwan. The MSI Cerius2 interface was used as a visualization and data analysis tool.

Dual-Level Direct Dynamics Calculation. We first give a brief introduction to the dual-level dynamics method employed in the present study since it is relatively new. Modeling large reacting systems is very difficult, and usually either the accuracy or the efficiency has to be sacrificed. In reaction rate constant calculation, the results are usually sensitive to the potential energy surface (PES) data used, and too much compromise in the accuracy of PES would result in severe errors. However, accurate rate constant calculation requires huge amount of PES information which usually is prohibitively expensive to obtain computationally at a single, very accurate level. To partially resolve this difficulty, a dual-level dynamics scheme has been proposed[18] and successfully applied to several systems.[1a,15b,18,19] In dual-level dynamics, the most important regions of the PES for dynamics calculation are calculated with high-level electronic structure theory. These important regions and the rest of the PES information as required by the dynamics methods are also calculated at a lower theoretical level. Since both high-level and low-level data are known at these pre-selected important regions, when PES data are needed at points between these pre-selected regions, interpolated corrections based on the low-level to high-level correction at the pre-selected region are applied to the low-level PES. For example, in the commonly used reaction-path method,[9,18] high-level calculation is performed at the important stationary points including the reactant, transition state, and product (or sometimes reaction complexes). A lower-level (much less resource-demanding) calculation is also performed to calculate the relevant region of the reaction-path. When PES data on the reaction path are need, an interpolated correction based on the high-level and low-level values at those stationary points is applied to the low-level data (energy, frequency, etc.) before they are used in the dynamics calculation. The advantage of the dual-level method is that one can concentrate on the most important regions of the PES with most of the available computational resource. If the low level calculation is qualitatively correct, the PES data after the interpolated correction should also be in good quality. After the high-level calculation is finished, the dynamics calculation can proceed with good efficiency. Thus, larger chemical systems can be modeled without significant compromise in accuracy.

In the current study, the reaction rate constants were calculated using the variational transition state theory at the canonical ensemble level (CVT),[20] which locates a single reaction bottleneck at every given temperature. The tunneling correction applied is the microcanonical optimized multidimensional tunneling (μOMT) method,[21] which takes the dominant tunneling probability between the small-curvature (SCT)[22] and the large-curvature tunneling (LCT)[22b,23] approaches at any given energies. The dual-level scheme[15b,18] mentioned above is used to incorporate the high-level electronic structure calculation data with the low-level PM3-SRP reaction path information. Using the dual-level notation,[15b] the direct dynamical method of the current study can be denoted as MP2/aug-cc-pVDZ [MP2/ADZP]///PM3-SRP, which means that the geometry and the energies are taken from the MP2/aug-cc-pVDZ calculation, the vibrational frequencies taken from MP2/ADZP calculation, and the low-level reaction-path calculated at PM3-SRP level. The correction on the reactant-side of the reaction path is based on the reactant-side ion−dipole complex.[18] Redundant internal coordinate system[24] was used in the vibrational analysis along the reaction path. The IVTST-0 method[18,25] is used for the lowest vibrational mode along the reaction path in the dual-level calculation. The reduced mass of the reaction is set to 1 amu, and the Page McIver method[26] is used

(10) (a) Bohme, D. K.; Raksit, A. B. *Can. J. Chem.* **1985**, *63*, 3007. (b) O'Hair, R. A. J.; Davico, G. E.; Hacaloglu, J.; Dang, T. T.; DePuy, C. H.; Bierbaum, V. M. *J. Am. Chem. Soc.* **1994**, *116*, 3609. (c) Viaggiano, A. A.; Arnold S. T.; Moris, R. A.; Ahrens, A. F.; Hierl, P. M. *J. Phys. Chem.* **1996**, *100*, 14397. (d) Seeley, J. V.; Morris, R. A.; Viggiano, A. A.; Wang, H.; Hase, W. L. *J. Am. Chem. Soc.* **1997**, *119*, 577. (e) Seeley, J. V.; Morris, R. A.; Viggiano, A. A. *J. Phys. Chem. A* **1997**, *101*, 4598. (f) Weis, P.; Kemper, P. R.; Bowers, M. T. *J. Am. Chem. Soc.* **1999**, *121*, 3531.

(11) (a) Tucker, S. C.; Truhlar, D. G. *J. Am. Chem. Soc.* **1990**, *112*, 3347. (b) Re, M.; Laria, D. *J. Chem. Phys.* **1996**, *105*, 4584. (c) Okuno, Y. *J. Chem. Phys.* **1996**, *105*, 5817.

(12) Hehre, W. J.; Radom, L.; Schleyer, P. v. R.; Pople, J. A. *Ab initio Molecular Orbital Theory*; Wiley: New York, 1986.

(13) Gaussian 94, Revision E.3, Frisch, M. J.; Trucks, G. W.; Schlegel, H. B.; Gill, P. M. W., Johnson, B. G.; Robb, M. A.; Cheeseman J. R.; Keith, T.; Petersson, G. A.; Montgomery, J. A.; Raghavachari, K.; Al-Laham, M. A.; Zakrzewski, V. G.; Ortiz, J. V.; Foresman, J. B.; Cioslowski, J.; Stefanov, B. B.; Nanayakkara, A.; Challacombe, M.; Peng, C. Y.; Ayala, P. Y.; Chen, W.; Wong, M. W.; Andres J. L.; Replogle E. S.; Gomperts, R.; Martin R. L.; Fox D. J.; Binkley J. S.; Defrees D. J.; Baker J.; Stewart, J. P.; Head-Gordon, M.; Gonzalez, C.; Pople, J. A. Gaussian, Inc.: Pittsburgh, PA, 1995.

(14) Stewart, J. J. P. *J. Comput. Chem.* **1989**, *10*, 221.

(15) (a) Gonzalez-Lafont, A.; Truong, T. N.; Truhlar, D. G. *J. Phys. Chem.* **1991**, *95*, 4618. (b) Corchado, J. C.; Espinosa-Garcia, Joaquin; Hu, W.-P.; Rossi, I.; Truhlar, D. G. *J. Phys. Chem.* **1995**, *99*, 687.

(16) (a) Dewar, M. J. S.; Zoebisch, E. G.; Healy, E. F.; Stewart, J. J. P. *J. Am. Chem. Soc.* **1985**, *107*, 3902. (b) Dewar, M. J. S.; Zoebisch, E. G. *J. Mol. Struct. (THEOCHEM)* **1988**, *180*, 1.

(17) Stewart, J. J. P.; Rossi, I.; Hu, W.-P.; Lynch, G. C.; Liu, Y.-P.; Truhlar, D. G. *MOPAC 5.07mn Program*; University of Minnesota: Minneapolis, 1997.

(18) Hu, W.-P.; Liu, Y.-P.; Truhlar, D. G. *J. Chem. Soc., Faraday Trans.* **1994**, *90*, 1715.

(19) Hu, W.-P.; Rossi, I.; Corchado, J. C.; Truhlar, D. G. *J. Phys. Chem. A* **1997**, *101*, 6911.

(20) (a) Garrett, B. C.; Truhlar, D. G. *J. Chem. Phys.* **1979**, *70*, 1593. (b) Garrett, B. C.; Truhlar, D. G. *J. Am. Chem. Soc.* **1979**, *101*, 4534.

(21) Liu, Y.-P.; Lu, D.-h.; Gonzalez-LaFont, A.; Truhlar, D. G.; Garrett, B. C. *J. Am. Chem. Soc.* **1993**, *115*, 7806.

(22) (a) Liu, Y.-P.; Lynch, G. C.; Truong, T. N.; Lu, D.-h.; Truhlar, D. G.; Garrett, B. C. *J. Am. Chem. Soc.* **1993**, *115*, 2408. (b) Lu, D.-h.; Truong, T. N.; Melissas, V. S.; Lynch, G. C.; Liu, Y.-P.; Garrett, B. C.; Steckler, R.; Isaacson, A. D.; Rai, S. N.; Hancock, G. C.; Lauderdale, J. G.; Joseph, T.; Truhlar, D. G. *Comput. Phys. Commun.* **1992**, *71*, 235.

(23) Garrett, B. C.; Joseph, T.; Truong, T. N.; Truhlar, D. G. *Chem. Phys.* **1989**, *136*, 271; **1990**, *140*, 207(E).

(24) Chuang, Y.-Y.; Truhlar, D. G. *J. Phys. Chem. A* **1998**, *102*, 242.

(25) Gonzalez-Lafont, A.; Truong, T. N.; Truhlar, D. G. *J. Chem. Phys.* **1991**, *95*, 8875.

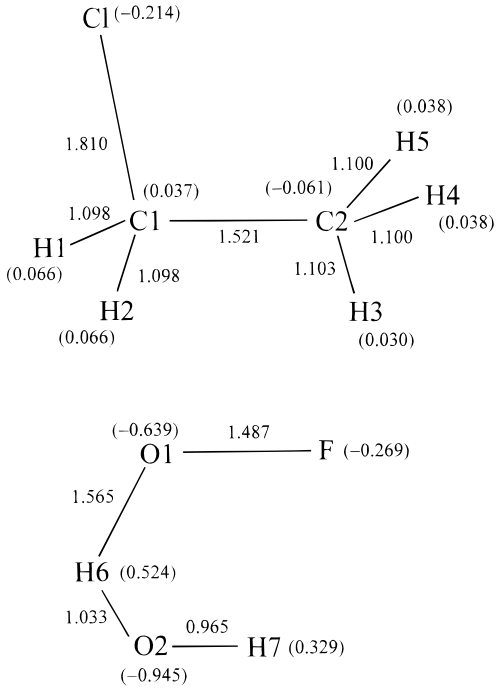

Figure 1. Calculated geometry of the reactants at MP2/aug-cc-pVDZ level. The bond lengths in the figure are in angstroms. The representative bond angles in degrees are C_2H_5Cl: Cl−C1−C2 110.8, H1−C1−H2 109.4, C1−C2−H3 109.4, H4−C2−H5 108.7; $OF^-(H_2O)$: F−O1−H6 94.4, O1−H6−O2 174.9, H6−O2−H7 100.6. Numbers in parentheses are ChelpG charges calculated from the MP2 density.

to calculate the reaction path with both the gradient and Hessian step sizes set to 0.002 b. The rate constant calculation was performed using a slightly modified version of MORATE 8.0[27] program on a SGI Octane workstation in our group.

Results

The calculated reactant and product geometry are depicted in Figures 1 and 2, and the transition state geometry in Figure 3. The calculated ChelpG[28] atomic charges with the MP2 density are also shown in Figures 1−3. The full set of optimized geometry parameters of all stationary points can be found in the Supporting Information. Table 1 gives the calculated reaction energies and the classical barrier heights at various levels, along with available experimental data.[29] The exact energy of reaction is estimated from: (1) the gas-phase thermodynamics data in ref 29, (2) the calculated zero-point and thermal energies at MP2/ADZP level, and (3) the calculated microsolvation energies with a single water molecule for OF^- and HOF at MP2/aug-cc-pVTZ level. The MP2/aug-cc-pVTZ method is chosen because it predicts a binding energy (ΔH_0°) of −26.9 kcal/mol for the flouride ion−water system, in very good agreement with a new experimentally determined value[10f] of −26.2 ± 0.8 kcal/mol. The PM3 parameters that were modified in our current PM3-SRP method are also listed in the footnote of Table 1. The classical barrier height calculated at MP2/aug-cc-pVDZ level is 4.4 kcal/mol. However, as in most reaction dynamics study, an accurate estimate of the barrier height is extremely difficult,

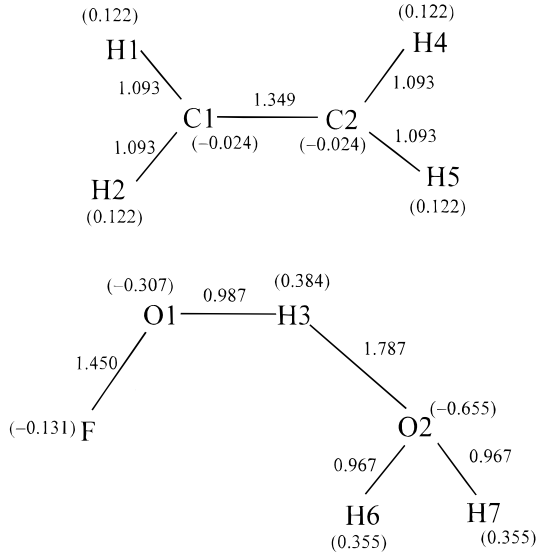

Figure 2. Calculated geometry of the products at MP2/aug-cc-pVDZ level. The bond lengths in the figure are in angstroms. The representative bond angles in degrees are C_2H_4: H1−C1−C2 121.4; $HOF(H_2O)$: F−O1−H3 97.0, O1−H3−O2 178.3, H3−O2−H6 112.2, H6−O2−H7 104.5. Numbers in parentheses are ChelpG charges calculated from the MP2 density.

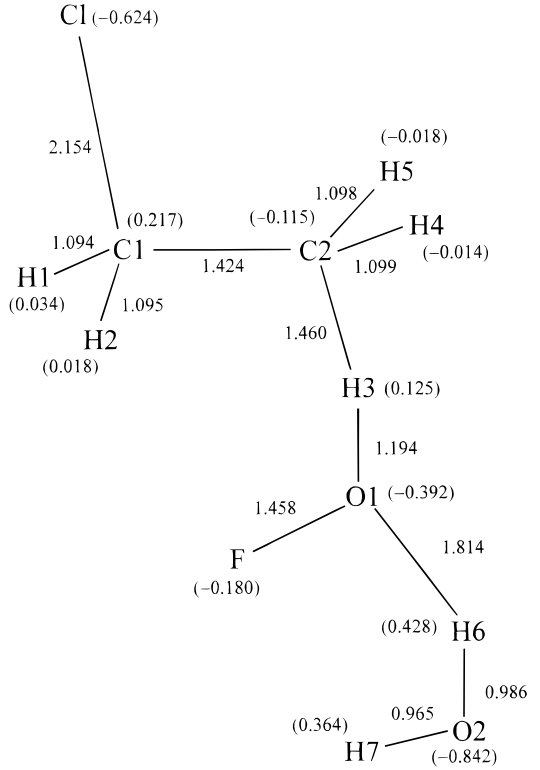

Figure 3. Calculated geometry of the E2 transition state at MP2/aug-cc-pVDZ level. The bond lengths in the figure are in angstroms. The representative bond angles in degrees are Cl−C1−C2 116.4, C1−C2−H3 100.3, C2−H3−O1 175.4, H3−O1−F 98.6, H1−C1−H2 113.1, H4−C2−H5 113.2, F−O1−H6 99.5, O1−H6−O2 172.4, H6−O2−H7 102.2. Numbers in parentheses are ChelpG charges calculated from the MP2 density.

especially in large systems. This is because there are many different sources of errors involved in the calculations, and most of the errors are more severe at transition states. For example, the incompleteness of the basis sets and the underestimation of the correlation energies of the MP2 method tend to make

(26) (a) Page, M.; McIver, J. W., Jr. *J. Chem. Phys.* **1988**, *88*, 922. (b) Page, M.; Doubleday: C.; McIver, J. W., Jr. *J. Chem. Phys.* **1990**, *93*, 5634.
(27) Chuang, Y.-Y.; Fast, P. L.; Hu, W.-P.; Lynch, G. C.; Liu, Y.-P.; Truhlar, D. G. *MORATE 8.0 Program*; Department of Chemistry and Supercomputer Institute, University of Minnesota: Minneapolis, 1998.
(28) Breneman, C. M.; Wiberg, K. B. *J. Comput. Chem.* **1990**, *11*, 361.
(29) Chase, M. W.; Jr.; Davies, C. A.; Downey, J. R., Jr.; Frurip, D. J.; McDonald, R. A.; Syverud, A. N. *J. Phys. Chem. Ref. Data* **1985**, *14*, Suppl. 1.

Table 1. Born−Oppenheimer Energies of Reaction and Barrier Heights (in kcal/mol) at Various Levels

	ΔE_{rxn}	$\Delta V^{\ddagger}$
MP2/6-31+G*	8.7	12.9
MP2/ADZP	6.3	8.6
MP2/aug-cc-pVDZ	3.6	4.4
PM3	2.4	2.1
PM3-SRP[a]	−1.2	4.4
experiment/estimated	−0.6[b]	3−5[c]

[a] PM3 parameters (in eV) changed in the current PM3-SRP method: U_{ss}(C), default value = −47.2703, new value = −42.78; U_{pp}(Cl), default value = −53.6144, new value = −54.00. [b] From gas-phase (without microsolvation) data in ref 28, calculated zero-point and thermal energies at MP2/ADZP level, and calculated microsolvation energies of OF^- and HOF at MP2/aug-cc-pVTZ level. [c] Estimated value based on MP2/aug-cc-pVDZ result and other factors, see text.

the calculation overestimate the barrier. However, the basis set superposition error (BSSE),[30,31] which we estimated using counterpoised (CP) calculations[31−33] to be around 4 kcal/mol at MP2/aug-cc-pVDZ level, tends to make the calculation underestimate the barrier. Furthermore, as seen in Table 1, the calculated Born−Oppenheimer energy of reaction at MP2/aug-cc-pVDZ level is about 4 kcal/mol higher than the available experimental value. This possibly would also lead to an overestimation of the barrier height. If we now assume that the effects of the BSSE and the barrier-overestimating factors almost cancel out with an uncertainty around 1 kcal/mol in either directions, we arrive at an estimated classical barrier height of 3−5 kcal/mol. Thus, in the dual-level dynamics calculation of the reaction rate constants, we used 3, 4, and 5 kcal/mol as the high-level classical barriers. (It is noted, however, the 1 kcal/mol uncertainty here is probably too optimistic at this level of theory even after considering the above correcting factors, and the uncertainty is mainly used for defining a convenient but also reasonable barrier range for calculating the rate constant and kinetic isotope effects. See the next section for further discussion.) Moreover, to obtain clearer trends of the tunneling contribution to the rate constants and KIEs as a function of barrier heights, we also did additional calculation with the classical barrier set to 6 kcal/mol. The high-level Born−Oppenheimer energy of reaction is set to the estimated value of −0.6 kcal/mol in the rate constant calculation. Table 2 shows the calculated vibrational frequencies of stationary points at the MP2/ADZP level which are used as high-level frequencies in the dual-level dynamics calculation.

The calculated conventional transition state theory (TST), canonical variational theory (CVT), and the canonical variational theory with microcanonical optimized multidimensional tunneling correction (CVT/μOMT) rate constants at various temperatures are summarized in Table 3. The calculated rate constants where the five hydrogen atoms on the ethyl chloride are replaced by deuterium are shown in Table 4. Table 5 gives the kinetic isotope effects (KIEs) due to this substitution. The calculated rate constants where the two hydrogen atoms on the water are replaced by deuterium are shown in Table 6 and the solvent kinetic isotope effects (SKIEs) due to this substitution are listed in Table 7. The calculated temperature dependence of the KIEs and SKIEs are plotted in Figures 4−6. The KIE or

Table 2. Calculated Vibrational Frequencies (in cm^{-1}) at MP2/ADZP Level

	C_2H_5Cl	OF^--(H_2O)	C_2H_4	HOF-(H_2O)	TS		TS
υ_1	3214	3899	3310	3949	3914	υ_{19}	719
υ_2	3193	2663	3285	3832	3585	υ_{20}	605
υ_3	3189	1788	3206	3567	3276	υ_{21}	586
υ_4	3132	1049	3187	1648	3218	υ_{22}	455
υ_5	3090	893	1688	1487	3180	υ_{23}	402
υ_6	1499	609	1467	924	3134	υ_{24}	300
υ_7	1492	316	1376	740	1719	υ_{25}	205
υ_8	1484	112	1236	299	1617	υ_{26}	164
υ_9	1410	102	1066	239	1548	υ_{27}	112
υ_{10}	1328		973	227	1457	υ_{28}	92
υ_{11}	1282		936	91	1312	υ_{29}	66
υ_{12}	1108		826	55	1263	υ_{30}	60
υ_{13}	1089				1259	υ_{31}	22
υ_{14}	1007				1176	υ_{32}	5
υ_{15}	792				1049	υ_{33}	696 *i*
υ_{16}	708				998		
υ_{17}	338				924		
υ_{18}	279				770		

SKIE can be further factorized into the translational, rotational, vibrational, variational, and the tunneling contributions

$$\mathrm{KIE} = \frac{k_H}{k_D} = \eta_{trans}\eta_{rot}\eta_{vib}\eta_{var}\eta_{tunneling} \quad (1)$$

The first four factors have been describe in earlier work,[1a,5,7,15] and the tunneling contribution is defined in the current study by

$$\eta_{tunneling} = \frac{k_H^{CVT/\mu OMT}/k_D^{CVT/\mu OMT}}{k_H^{CVT}/k_D^{CVT}} \quad (2)$$

This is the factor to be multiplied by the classically calculated (CVT) KIEs and SKIEs to obtain the tunneling corrected KIEs and SKIEs. These contributions at different temperatures are reported in Tables 8 and 9.

Discussion

Geometry and Charges. We see from Figures 1−3 that the calculated carbon−carbon bond distances decrease from 1.521 Å (single bond) at the reactant (ethyl chloride) to 1.424 Å at the transition state, and to 1.349 Å (double bond) at the product (ethene). This is in reasonably good agreement with experimental ethene C−C bond distance of 1.337 Å. The C−C bond distance at the transition state is roughly mid-way between the reactant and the product, which is usually the case for a nearly isoergic reaction. The C−Cl and C2−H3 (H3 is the hydrogen atom being abstracted) bond distances increase by 0.344 and 0.357 Å, respectively, from the reactant to the transition state. It is noted that the chlorine atom has developed a significant negative charge (−0.624) at the transition state. The distance between the abstracted hydrogen (H3) and the hydrogen acceptor (O1) at the transition state is 1.194 Å, which is only 0.207 Å longer than the corresponding O−H distance of the product. It is also interesting to compare the bond distances of those bonds that are involved in hydrogen bonding, most importantly, the O1−H6 and H6−O2 bonds. The O1−H6 distance at the reactant is 1.565 Å, and it increases to 1.814 Å at the transition state. This implies a significant decrease in the hydrogen bonding (or microsolvation) strength, as will be discussed later in this section. The H6−O2 bond distance is also an indicator of the hydrogen bonding strength since the electron density along the H6−O2 bond is drawn to the O1−H6 hydrogen bonding. Thus,

(30) Morokuma, K.; Kitaura, K. In *Chemical Applications of Atomic and Molecular Electrostatic Potential*; Politzer, P., Truhlar, D. G., Eds.; Plenum: New York, 1981; p 215.
(31) Boys, S. F.; Bernardi, F. *Mol. Phys.* **1970**, *17*, 553.
(32) Schwenke, D. W.; Truhlar, D. G. *J. Chem. Phys.* **1985**, *82*, 2418; **1987**, *86*, 3760 (E).
(33) Simon, S.; Duran, M.; Dannenberg, J. J. *J. Phys. Chem. A* **1999**, *103*, 1640.

Table 3. Calculated Rate Constants (in cm^3 $molecule^{-1}$ s^{-1}) of the $C_2H_5Cl + OF^-(H_2O)$ Reaction

	$V^{\ddagger}$= 3 kcal/mol			$V^{\ddagger}$= 4 kcal/mol		
T (K)	TST	CVT	CVT/μOMT	TST	CVT	CVT/μOMT
200	7.52 (−14)[a]	6.41 (−14)	8.94 (−14)	6.08 (−15)	5.18 (−15)	4.60 (−14)
250	1.53 (−13)	1.33 (−13)	1.65 (−13)	2.05 (−14)	1.77 (−14)	8.50 (−14)
300	2.80 (−13)	2.44 (−13)	2.84 (−13)	5.22 (−14)	4.57 (−14)	1.48 (−13)
400	7.56 (−13)	6.67 (−13)	7.26 (−13)	2.15 (−13)	1.90 (−13)	3.94 (−13)
500	1.69 (−12)	1.50 (−12)	1.58 (−12)	6.18 (−13)	5.49 (−13)	8.98 (−13)
600	3.33 (−12)	2.96 (−12)	3.06 (−12)	1.44 (−12)	1.28 (−12)	1.82 (−12)
800	9.87 (−12)	8.79 (−12)	8.95 (−12)	5.26 (−12)	4.69 (−12)	5.75 (−12)
	$V^{\ddagger}$= 5 kcal/mol			$V^{\ddagger}$= 6 kcal/mol		
T (K)	TST	CVT	CVT/μOMT	TST	CVT	CVT/μOMT
200	4.91 (−16)	4.19 (−16)	2.39 (−14)	3.96 (−17)	3.39 (−17)	1.22 (−14)
250	2.73 (−15)	2.37 (−15)	4.51 (−14)	3.65 (−16)	3.17 (−16)	2.33 (−14)
300	9.76 (−15)	8.54 (−15)	8.04 (−14)	1.82 (−15)	1.60 (−15)	4.23 (−14)
400	6.11 (−14)	5.39 (−14)	2.23 (−13)	1.74 (−14)	1.53 (−14)	1.22 (−13)
500	2.26 (−13)	2.01 (−13)	5.31 (−13)	8.26 (−14)	7.33 (−14)	3.05 (−13)
600	6.22 (−13)	5.53 (−13)	1.12 (−12)	2.69 (−13)	2.39 (−13)	6.71 (−13)
800	2.80 (−12)	2.50 (−12)	3.79 (−12)	1.50 (−12)	1.33 (−12)	2.45 (−12)

[a] 7.52 (−14) means 7.52×10^{-14}.

Table 4. Calculated Rate Constants (in cm^3 $molecule^{-1}$ s^{-1}) of the $C_2D_5Cl + OF^-(H_2O)$ Reaction

	$V^{\ddagger}$= 3 kcal/mol			$V^{\ddagger}$= 4 kcal/mol		
T (K)	TST	CVT	CVT/μOMT	TST	CVT	CVT/μOMT
200	5.71 (−15)	5.11 (−15)	2.87 (−14)	4.61 (−16)	4.13 (−16)	9.82 (−15)
250	1.87 (−14)	1.68 (−14)	5.63 (−14)	2.50 (−15)	2.25 (−15)	2.06 (−14)
300	4.73 (−14)	4.27 (−14)	1.04 (−13)	8.84 (−15)	7.98 (−15)	4.06 (−14)
400	1.95 (−13)	1.76 (−13)	3.02 (−13)	5.55 (−14)	5.02 (−14)	1.33 (−13)
500	5.69 (−13)	5.14 (−13)	7.34 (−13)	2.08 (−13)	1.88 (−13)	3.59 (−13)
600	1.34 (−12)	1.21 (−12)	1.55 (−12)	5.78 (−13)	5.22 (−13)	8.24 (−13)
800	4.94 (−12)	4.45 (−12)	5.15 (−12)	2.64 (−12)	2.37 (−12)	3.09 (−12)
	$V^{\ddagger}$= 5 kcal/mol			$V^{\ddagger}$= 6 kcal/mol		
T (K)	TST	CVT	CVT/μOMT	TST	CVT	CVT/μOMT
200	3.72 (−17)	3.34 (−17)	3.53 (−15)	3.01 (−18)	2.70 (−18)	1.30 (−15)
250	3.33 (−16)	3.00 (−16)	7.67 (−15)	4.45 (−17)	4.01 (−17)	2.88 (−15)
300	1.65 (−15)	1.49 (−15)	1.58 (−14)	3.09 (−16)	2.79 (−16)	6.16 (−15)
400	1.58 (−14)	1.43 (−14)	5.77 (−14)	4.49 (−15)	4.06 (−15)	2.46 (−14)
500	7.60 (−14)	6.87 (−14)	1.71 (−13)	2.78 (−14)	2.51 (−14)	8.02 (−14)
600	2.50 (−13)	2.26 (−13)	4.28 (−13)	1.08 (−13)	9.75 (−14)	2.18 (−13)
800	1.41 (−12)	1.26 (−12)	1.82 (−12)	7.49 (−13)	6.74 (−13)	1.06 (−12)

the stronger O1−H6 hydrogen bonding is, the longer the H6−O2 bond distance. As also seen in the Figures, the H6−O2 distance is 1.033 Å at the reactant, which corresponds to a strong hydrogen bond, and it decreases to 0.986 Å at the transition state, and then further decreases to 0.967 Å at the product. (As seen in Figure 2, the H6 atom does not directly involve hydrogen bonding in the product.) As a comparison, the calculated bond length of a free water molecule at the same level (MP2/aug-cc-pVDZ) is 0.966 Å. The above bond distance data correspond well to the calculated microsolvation energies (Born−Oppenheimer energies, not including the zero-point and thermal excitation energies) of −22.3, −13.3, and −8.6 kcal/mol for OF^-, transition state, and HOF, respectively, at the MP2/ADZP level. The decrease in the solvation energies from the reactant to the transition state is also implied by the charge distribution. As shown in Figures 1 and 3 that the total ChelpG charge on the OF^- ion is −0.908 while in the transition state the charge on the OF^- group is only −0.572. Significant charge delocalization has occurred from the reactant to the transition state. It also seems from Figures 1−3 that even though the E2 reaction involves a "proton transfer", the H3 atom never carries a very significant positive charge from the reactant to the product.

Table 5. Calculated Kinetic Isotope Effects [Ratios of the Rate Constants between $C_2H_5Cl + OF^-(H_2O)$ and $C_2D_5Cl + OF^-(H_2O)$ Reactions] at Various Levels of Theory

	$V^{\ddagger}$= 3 kcal/mol			$V^{\ddagger}$= 4 kcal/mol	
T (K)	TST[a]	CVT	CVT/μOMT	CVT	CVT/μOMT
200	13.2	12.5	3.11	12.5	4.68
250	8.18	7.92	2.93	7.87	4.13
300	5.92	5.71	2.73	5.73	3.65
400	3.88	3.79	2.40	3.78	2.96
500	2.97	2.92	2.15	2.92	2.50
600	2.49	2.45	1.97	2.45	2.21
800	2.00	1.98	1.74	1.98	1.86
	$V^{\ddagger}$= 5 kcal/mol			$V^{\ddagger}$= 6 kcal/mol	
T (K)		CVT	CVT/μOMT	CVT	CVT/μOMT
200		12.5	6.77	12.6	9.38
250		7.90	5.88	7.91	8.09
300		5.73	5.09	5.73	6.87
400		3.77	3.86	3.77	4.96
500		2.93	3.11	2.92	3.80
600		2.45	2.62	2.45	3.08
800		1.98	2.08	1.97	2.31

[a] The KIEs calculated by TST method are theoretically independent of barrier heights; therefore, only the 3 kcal/mol case is listed in the table.

Table 6. Calculated Rate Constants (in cm^3 $molecule^{-1}$ s^{-1}) of the $C_2H_5Cl + OF^-(D_2O)$ Reaction

	$V^{\ddagger}$= 3 kcal/mol			$V^{\ddagger}$= 4 kcal/mol		
T (K)	TST	CVT	CVT/μOMT	TST	CVT	CVT/μOMT
200	9.93 (−14)	8.75 (−14)	1.01 (−13)	8.02 (−15)	7.08 (−15)	4.83 (−14)
250	1.93 (−13)	1.71 (−13)	1.88 (−13)	2.58 (−14)	2.29 (−14)	9.06 (−14)
300	3.43 (−13)	3.05 (−13)	3.25 (−13)	6.40 (−14)	5.70 (−14)	1.60 (−13)
400	8.88 (−13)	7.92 (−13)	8.22 (−13)	2.52 (−13)	2.25 (−13)	4.25 (−13)
500	1.92 (−12)	1.72 (−12)	1.76 (−12)	7.03 (−13)	6.29 (−13)	9.64 (−13)
600	3.68 (−12)	3.29 (−12)	3.34 (−12)	1.59 (−12)	1.42 (−12)	1.93 (−12)
800	1.04 (−11)	9.31 (−12)	9.40 (−12)	5.57 (−12)	4.97 (−12)	5.93 (−12)
	$V^{\ddagger}$= 5 kcal/mol			$V^{\ddagger}$= 6 kcal/mol		
T (K)	TST	CVT	CVT/μOMT	TST	CVT	CVT/μOMT
200	6.48 (−16)	5.72 (−16)	2.52 (−14)	5.24 (−17)	4.62 (−17)	1.27 (−14)
250	3.45 (−15)	3.06 (−15)	4.84 (−14)	4.61 (−16)	4.09 (−16)	2.47 (−14)
300	1.20 (−14)	1.07 (−14)	8.72 (−14)	2.24 (−15)	1.99 (−15)	4.55 (−14)
400	7.17 (−14)	6.40 (−14)	2.43 (−13)	2.04 (−14)	1.82 (−14)	1.33 (−13)
500	2.57 (−13)	2.30 (−13)	5.73 (−13)	9.40 (−14)	8.40 (−14)	3.29 (−13)
600	6.88 (−13)	6.14 (−13)	1.19 (−12)	2.97 (−13)	2.66 (−13)	7.15 (−13)
800	2.97 (−12)	2.65 (−12)	3.92 (−12)	1.58 (−12)	1.41 (−12)	2.54 (−12)

Table 7. Calculated Solvent Kinetic Isotope Effects [Ratios of the Rate Constants between $C_2H_5Cl + OF^-(H_2O)$ and $C_2D_5Cl + OF^-(H_2O)$ Reactions] at Various Levels of Theory

	$V^{\ddagger}$= 3 kcal/mol			$V^{\ddagger}$= 4 kcal/mol	
T (K)	TST[a]	CVT	CVT/μOMT	CVT	CVT/μOMT
200	0.757	0.733	0.885	0.732	0.952
250	0.793	0.778	0.878	0.773	0.938
300	0.816	0.800	0.874	0.802	0.925
400	0.851	0.842	0.883	0.844	0.927
500	0.880	0.872	0.898	0.873	0.932
600	0.905	0.900	0.916	0.901	0.943
800	0.949	0.944	0.952	0.944	0.970
	$V^{\ddagger}$= 5 kcal/mol			$V^{\ddagger}$= 6 kcal/mol	
T (K)		CVT	CVT/μOMT	CVT	CVT/μOMT
200		0.733	0.948	0.734	0.961
250		0.775	0.932	0.775	0.943
300		0.798	0.922	0.804	0.930
400		0.842	0.918	0.841	0.917
500		0.874	0.927	0.873	0.927
600		0.901	0.941	0.898	0.938
800		0.943	0.967	0.943	0.965

[a] The SKIEs calculated by TST method are theoretically independent of barrier heights; therefore, only the 3 kcal/mol case is listed in the table.

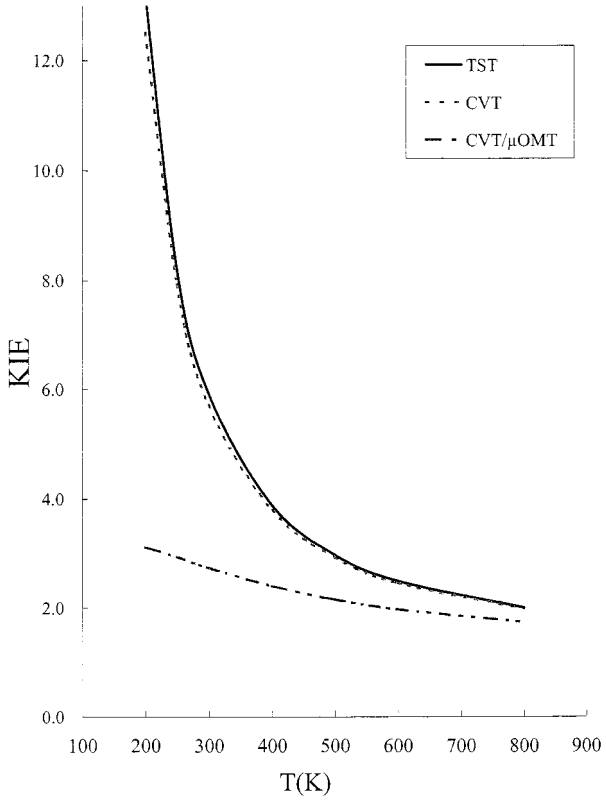

Figure 4. Temperature dependence of the calculated KIEs with a classical barrier height of 3 kcal/mol.

Reaction Energetics and Barrier Height. In Table 1 we see that the energies of reaction calculated by MP2/aug-cc-pVDZ methods are in reasonably good agreement with the experimental value, considering the size of the system. In the present study we assume that one of the products is the solvated HOF molecule. In principle, a solvated chloride ion is also possible and more thermodynamically favored. However, reaction path calculation at PM3-SRP and MP2/ADZP levels showed that the water stayed with the HOF molecule long after passing the transition state. Thus, it seems that at least the initial product of the reaction is $HOF(H_2O)$ molecule, and the $Cl^-(H_2O)$ ion could be formed in subsequent collisions.

The highest level of transition state geometry optimization is at the MP2/aug-cc-pVDZ level, and the calculated classical barrier height is 4.4 kcal/mol. As discussed in the previous section, after considering several sources of errors, the classical barrier height is estimated to be 3−5 kcal/mol. As shown in Table 1, we slightly modified two of the PM3 parameters to obtain a PM3-SRP potential energy surface which agrees better with experimental energetics and with our estimated classical barrier height. This PM3-SRP method serves as the low-level potential energy surface in our dual-level dynamics calculation.

Vibrational Frequencies. Due to the resource limitation, the harmonic frequencies of the stationary points were calculated at the MP2/ADZP level (on the geometry optimized at the same level) instead of the MP2/aug-cc-pVDZ level. As seen in Table 2 one of the C−H stretching frequency (around 3100 cm^{-1}) of C_2H_5Cl turns into a much lower-frequency symmetric stretching mode (at 1548 cm^{-1}) between the two reactants. (The 1548 cm^{-1} mode was assigned by animating all of the vibrational modes of the transition state at the MP2/ADZP level.) As will be discussed later, this decrease is the main contribution to the normal KIEs of the reaction. It is also noted that in the reactant $OF^-(H_2O)$, one of the O−H stretching frequencies, 2663 cm^{-1},

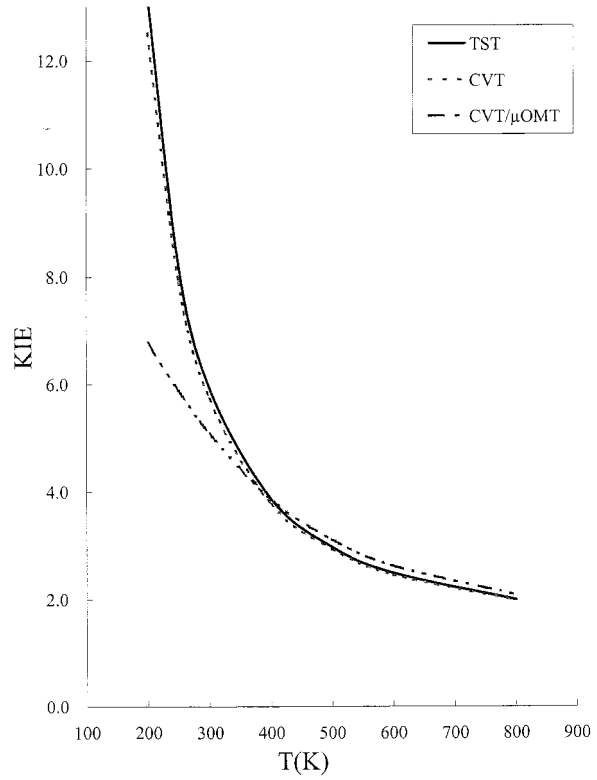

Figure 5. Temperature dependence of the calculated KIEs with a classical barrier height of 5 kcal/mol.

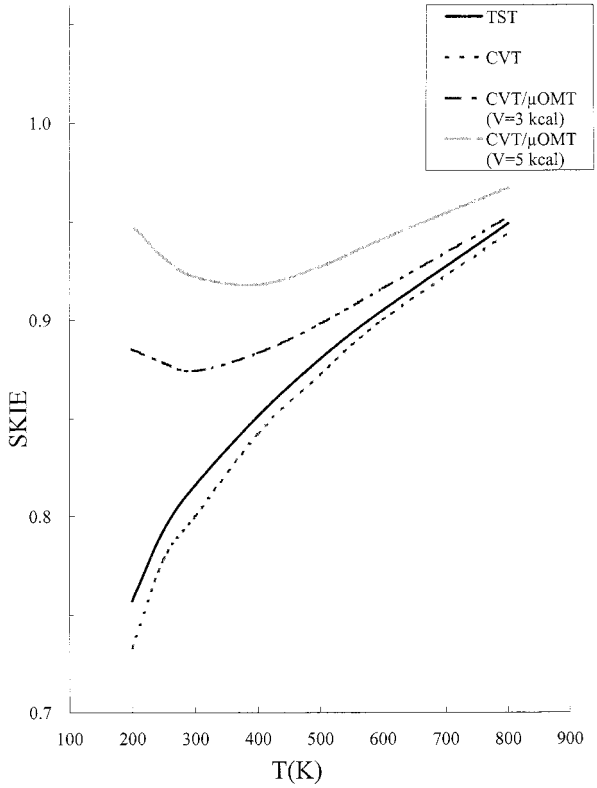

Figure 6. Temperature dependence of the calculated SKIEs with classical barrier heights of 3 and 5 kcal/mol. Since the calculated SKIEs by the TST and CVT methods are virtually independent of barrier heights, only the 3 kcal/mol case is plotted for these two methods.

is much lower than the values in free water molecules (which at MP2/ADZP level are 3963 and 3842 cm^{-1}). This dramatic lowering of frequency is due to the strong hydrogen bonding to the OF^- ion. However, the microsolvation at the transition state is much weaker, and the frequency increases to 3585 cm^{-1}. This also corresponds well to the calculated microsolvation energy of −22.3 and −12.1 kcal/mol (at the MP2/ADZP level) for OF^- and the transition state, respectively. As will be discussed later, this difference in solvent vibrational frequency is one of the major contributions to the inverse solvent kinetic isotope effects (SKIEs). As also seen in Table 2, there are several very low-frequency modes at the transition states, which indicate very floppy transition structures. These modes would have been better treated as hindered rotors[19,34] in the rate constant calculation. However, the current version of the MORATE program does not support any anharmonic treatment when using the nonredundant internal coordinates. If future work is to make quantitative comparison between the theoretical prediction to the experimental rate constants, the hindered-rotor approximation should somehow be applied, especially at higher temper-

Table 8. Factor[a]Analysis of the Calculated KIEs

	$V^{\ddagger}$= 3 kcal/mol			$V^{\ddagger}$= 4 kcal/mol	
T (K)	η_{vib}[b]	η_{var}	$\eta_{tunneling}$	η_{var}	$\eta_{tunneling}$
200	9.02	0.952	0.248	0.951	0.373
250	5.60	0.968	0.370	0.959	0.525
300	4.06	0.965	0.478	0.970	0.637
400	2.66	0.978	0.634	0.977	0.783
500	2.03	0.983	0.738	0.983	0.857
600	1.70	0.984	0.807	0.984	0.901
800	1.37	0.989	0.880	0.993	0.940

	$V^{\ddagger}$= 5 kcal/mol		$V^{\ddagger}$= 6 kcal/mol	
T (K)	η_{var}	$\eta_{tunneling}$	η_{var}	$\eta_{tunneling}$
200	0.951	0.540	0.954	0.747
250	0.964	0.744	0.964	1.023
300	0.969	0.888	0.974	1.197
400	0.975	1.025	0.972	1.316
500	0.984	1.061	0.983	1.302
600	0.984	1.069	0.984	1.256
800	0.999	1.050	0.985	1.171

[a] The translational and rotational contributions are independent of temperatures and barrier heights and are 1.051 and 1.389, respectively. [b] The vibrational contributions are independent of barrier heights; therefore, only the 3 kcal/mol case is listed in the table.

Table 9. Factor[a]Analysis of the Calculated SKIEs

	$V^{\ddagger}$= 3 kcal/mol			$V^{\ddagger}$= 4 kcal/mol	
T (K)	η_{vib}[b]	η_{var}	$\eta_{tunneling}$	η_{var}	$\eta_{tunneling}$
200	0.712	0.967	1.208	0.965	1.302
250	0.745	0.981	1.128	0.973	1.214
300	0.767	0.980	1.092	0.983	1.154
400	0.800	0.989	1.049	0.990	1.098
500	0.827	0.991	1.029	0.993	1.067
600	0.850	0.994	1.018	0.995	1.046
800	0.892	0.995	1.008	0.999	1.028

	$V^{\ddagger}$= 5 kcal/mol		$V^{\ddagger}$= 6 kcal/mol	
T (K)	η_{var}	$\eta_{tunneling}$	η_{var}	$\eta_{tunneling}$
200	0.967	1.295	0.971	1.309
250	0.979	1.203	0.979	1.217
300	0.981	1.155	0.990	1.156
400	0.988	1.090	0.986	1.091
500	0.994	1.060	0.993	1.062
600	0.996	1.045	0.992	1.044
800	1.001	1.025	0.994	1.023

[a] The translational and rotational contributions are independent of temperatures and barrier heights and are 1.031 and 1.032, respectively. [b] The vibrational contributions are independent of barrier heights; therefore, only the 3 kcal/mol case is listed in the table.

(34) Truhlar, D. G. *J. Comput. Chem.* **1991**, *12*, 266.

atures. Short evaluation of the anharmonic effects to the calculated KIEs and SKIEs is included at the end of this section.

Rate Constants. In Tables 3, 4, and 6 we see that in all cases CVT rate constants are only slightly less than TST rate constants. The variational effects (differences between the CVT and TST) are small (<20%) in the current system. As seen in Table 3, the tunneling has only modest contribution to the perprotic rate constants when the barrier is 3 kcal/mol. However, when the barrier is 4 kcal/mol or above, the tunneling dominates the rate constants below 400 K. For example, at 300 K, the rate constants calculated with tunneling correction are 1.2, 3.2, 9.4, and 26 times the CVT values for the 3, 4, 5, and 6 kcal/mol barrier cases, respectively. Arrhenius plots of the rate constants are included in the Supporting Information.

In the pentadeuterated ethyl chloride reaction, however, tunneling is important even when the barrier is only 3 kcal/mol, as can be seen in Table 4. At the same temperature and with the same classical barrier heights, all of the calculated rate constants are *lower* than those of the perprotic reaction. This is because the pentadeuterated reaction has a higher zero-point corrected barrier. This will be further discussed later in this section.

As shown in Tables 3 and 6, if the microsolvent H_2O molecule is replaced by D_2O, the rate constants *increase* slightly, by 5−27% at CVT level and by 4−12% at CVT/μOMT level. Compared to the D_2O reaction, tunneling is slightly more important in the H_2O reaction. This is because the H_2O reaction has a higher zero-point corrected barrier. This will also be further discussed later in this section.

In the current study, the small-curvature tunneling is the dominating tunneling mechanism at all energies.

Kinetic Isotope Effects (KIEs). One of the primary goals of this study is to understand the tunneling contribution to the KIEs. E2 reactions have been known to exhibit normal KIEs. This can be understood if one recognizes that a strong C−H bond is broken during the reaction. From the reactant to the transition state, a high-frequency C−H stretching mode (around 3100−3200 cm^{-1}) turns into a medium-frequency (in the current system, 1548 cm^{-1}) hydrogen atom symmetric stretching between C2 and O1 atoms. (Actually, our simulation showed that this mode also correlates strongly to the change in C1−C2 bond distance.) This amounts to approximately a 1600 cm^{-1} reduction in the vibrational frequency and thus an 800 cm^{-1} reduction in the zero-point energy. However, in the pentadeuterated reaction, this mode decreases from around 2300 cm^{-1} at the reactant to 1372 cm^{-1} at the transition state. The corresponding decrease in the vibrational frequency is about 900 cm^{-1} and the decrease in the zero-point energy is about 450 cm^{-1}, which is about 350 cm^{-1} less than that of the perprotic reaction. Thus, the effective barrier for the pentadeuterated reaction is higher, and the reaction constants are thus lower, and normal KIEs are obtained. In the current study, the effective barrier for the pentadeuterated reaction is 0.9 kcal/mol higher than the perprotic reaction, and the vibrational mode mentioned above is the most important contribution to this difference.

However, we have been wondering if the tunneling may also contribute significantly to the KIEs when the reaction barrier is high since hydrogen should tunnel more readily than deuterium. As clearly shown in Table 5 and Figure 4, when the barrier is 3 kcal/mol, the KIEs calculated at the CVT/μOMT level are significantly *smaller* than those at the CVT level in most cases. That is, the tunneling contribute *inversely* to the KIEs. This result may at first seem puzzling, but it can be understood as follows. In Table 5, the calculated TST and CVT KIEs are all normal, ranging from about 13 at 200 K to 2 at 800 K. When the barrier is low, the tunneling increases the rate constants of the perprotic reaction only slightly. However, there is significant tunneling in the pentadeuterated reaction since it has a higher effective barrier. For example in the 3 kcal/mol barrier case, the tunneling increases the pentadeuterated rate constant by a factor of 5.6 at 200 K and 2.4 at 300 K, while in the perprotic reaction there is only about 20−40% increase. Thus, the tunneling significantly reduces the KIEs calculated by CVT. For example, at 300 K, the KIE calculated by CVT is 5.7 but it reduces to 2.7 by the CVT/μOMT method. At higher temperatures, the zero-point energy effects are less important, and thus the calculated KIEs by the CVT method decreases as temperature increases. The tunneling contribution to the rate constants also becomes less pronounced at higher temperatures, and thus the KIEs calculated by the CVT/μOMT method are similar to the CVT values. As seen in Table 8, the normal KIEs are contributed by the vibrations (or the zero-point energies), but the KIEs are lowered considerably at lower temperatures when tunneling is considered. The variational effects have slightly inverse contribution to the KIEs in all cases.

When there is a higher barrier, for example, in the 5 kcal/mol case, the tunneling contributions are important at all temperatures under study for both perprotic and pentadeuterated reactions. At low temperatures, virtually all of the rate constants are contributed by tunneling, as seen in Tables 3 and 4. The KIEs calculated by the CVT/μOMT method are approximately equal to the ratio of the amounts of tunneling of the two reactions. The hydrogen atom in the perprotic reaction *does* tunnel more than the deuterium atom in the pentadeuterated reaction, but it turns out that the ratio is smaller than the KIEs calculated by the CVT method. Thus, as shown in Table 8, the tunneling contribution to the KIEs at lower temperatures is also inverse. As the temperature increases, the CVT rate constants of the pentadeuterated reaction increase faster than those of the perprotic reaction since the pentadeuterated reaction has a higher effective barrier. As a result, the KIE values calculated by the CVT method decrease very rapidly as temperature increases. However, the ratio of the amounts of tunneling between these two reactions decreases more slowly than the KIEs calculated by CVT as the temperature becomes higher. For example, in the 5 kcal/mol barrier case, the CVT KIE at 200 K is 12.5, and it decreases to 2.9 at 500 K. The ratio of the amounts of tunneling between the perprotic and pentadeuterated reactions are 6.7 at 200 K and 3.2 at 500 K. Thus, as seen in Table 5 and Figure 5, the tunneling actually *increases* the CVT KIEs at higher temperatures. This can also be seen in Table 8 that in the high barrier cases (5 and 6 kcal/mol), the tunneling contribution to the KIEs becomes normal (>1.0) at higher temperatures. It is also noted in Table 5 that the KIEs calculated by the CVT method at a particular temperature are almost independent of the barrier height. However, when the tunneling effects are taken into account, the KIEs are functions of both temperatures and barrier heights.

Solvent Kinetic Isotope Effects (SKIEs). In the previous study[7] of a microsolvated S_N2 reaction, we have demonstrated that the change in the hydrogen bonding strength, or more specifically, the change in the O−H vibrational frequencies of the solvent, from the reactant to the transition state, is responsible for the experimentally observed[10b] inverse SKIEs. The current study is, to our knowledge, the first theoretical investigation including the tunneling effects on the SKIEs of a microsolvated E2 reaction. As mentioned earlier in this section,

there is a 922 cm^{-1} increase in one of the O−H vibrational frequencies of $OF^-(H_2O)$ from the reactant to the transition state. When the H_2O is replaced by D_2O, the corresponding frequency change is from 1946 cm^{-1} to 2603 cm^{-1} . These values are compared to the calculated O−D stretching frequencies of 2902 and 2772 cm^{-1} in a free D_2O molecule at MP2/ADZP level. The frequency increase in the D_2O reaction is 657 cm^{-1}, which is 265 cm^{-1} less than in the H_2O reaction. As a result, the effective barrier for the D_2O reaction is *lower*, and inverse SKIEs are obtained. (As in the previous study,[7,8] the transitional modes, which are the five lowest-frequency modes at the transition state that become translational and rotational motion at the reactant and product in this system, also contribute, but to a lesser extent, to the inverse SKIEs. The medium-frequency modes contribute normally to the SKIEs.) We can see in Table 7 that the SKIEs calculated at the TST or CVT levels at 300 K are 0.80−0.82 and are almost independent of the barrier heights. This is compared to the perfectly agreed theoretical and experimental values[7,10b] of 0.65 for the microsolvated S_N2 reaction of $F^-(H_2O) + CH_3Cl$.

However, when tunneling is included in the calculation, the calculated SKIEs increase by 10−15%, as can be seen in Table 7 and Figure 6. The increase is smaller for the 3 kcal/mol barrier case. This can be explained as follows. When the barrier is 3 kcal/mol, the H_2O reaction tunnels more than the D_2O reaction because the H_2O reaction has a higher effective barrier to tunneling through. (Effective barriers are 0.38 and 0.22 kcal/mol for H_2O and D_2O reactions, respectively.) This can be seen in Tables 3 and 6 that at 300 K tunneling increases the rate by 16% in the H_2O reaction but only 7% in the D_2O reaction. Thus, the tunneling makes a normal contribution to the SKIEs in that it increases the SKIE from 0.80 (CVT) to 0.87 (CVT/μOMT) at 300 K.

When the barrier is higher, tunneling dominates the rate constants at lower temperatures, and the SKIEs are thus approximately the ratio of the amounts of tunneling. However, when the barrier is higher than 3 kcal/mol, the D_2O reaction tunnels slightly *more* than the H_2O reaction. This can be understood that the atom that tunnels through the barrier is hydrogen in *both* reactions, but the effective barrier is lower for the D_2O reaction. When the barrier becomes higher, the amount of tunneling in the D_2O reaction will catch up with that in the H_2O reaction. As a result, inverse SKIEs are still obtained in higher-barrier cases. However, the tunneling ratio is slightly higher than the SKIE obtained by CVT method, and thus tunneling also contributes normally to the SKIE. In conclusion, the tunneling always contributes normally to the SKIEs (that is, makes the SKIE larger), as seen in Table 9, but for different reasons in low- and high-barrier cases.

Error Assessment. Considering the relatively large size of the system and various approximate methods employed in the calculation, it seems appropriate to discuss the effects due to a few potentially important sources of errors. First of all, the levels of electronic structure calculation (MP2/ADZP and MP2/aug-cc-pVDZ) used in the current study can only provide semi-quantitative information of the potential energy surface. The geometry and high-frequency vibrations are probably more converged than the reaction barrier height and the low-frequency modes. The estimated range of barrier height, 3−5 kcal/mol, might still be too narrow as compared to the average errors at these levels. However, as a model E2 system where tunneling and solvation effects are important, the calculation did demonstrate the trends in KIEs and SKIEs as functions of temperature in the modeled barrier height range.

Table 10. Calculated Vibrational Frequencies (in cm^{-1}) of the Transitional Modes

	TS of C_2H_5Cl + $OF^-(H_2O)$	TS of C_2D_5Cl + $OF^-(H_2O)$	TS of C_2H_5Cl + $OF^-(D_2O)$
ν_{28}	92.4	88.7	87.1
ν_{29}	66.2	64.7	62.2
ν_{30}	60.1	56.7	59.1
ν_{31}	22.0	21.4	21.0
ν_{32}	5.4	4.9	5.4

Table 11. Calculated Vibrational Contributions to KIEs and SKIEs of the Transitional Modes with Harmonic and Hindered Rotor Approximation

	KIEs		SKIEs	
T (K)	η_{har}	$\eta_{hin-rot}$	η_{har}	$\eta_{hin-rot}$
200	0.775	0.783	0.820	0.820
300	0.776	0.792	0.822	0.822
500	0.777	0.807	0.823	0.822
800	0.777	0.823	0.823	0.822

Additionally, harmonic treatment of the low-frequency modes raises concern on the accuracy of the calculated KIEs and SKIEs. Table 10 lists the frequencies of the transitional modes of the perprotic and the two deuterated transition states. It can be seen in the table that these frequencies are relatively insensitive to the isotopic substitutions as compared to the high-frequency modes as discussed earlier. It is not surprising since these modes correspond mostly to torsional motions among different structural subunits of the transition state. Table 11 shows the total vibrational contributions of these modes to the KIEs and SKIEs from 200 to 800 K by means of the harmonic treatment and one of the hindered rotor approximations by Truhlar.[34] For the contributions to the KIEs, the hindered rotor method predicts slightly higher (1−6%) values, while for the SKIEs the two methods agree within 0.2%. All of the contributions are not very temperature-dependent. Thus, it seems that no significant errors have been introduced to the vibrational contributions due to the harmonic approximation. It is also noted that in the current study the trends in the calculated KIEs and SKIEs are *not* determined by the low-frequency modes. From Tables 8 and 9 and detailed vibrational analysis[35] we found that the tunneling effects and the *high-frequency* modes dominate the contribution to the KIEs and SKIEs. (The temperature-independent rotational contribution to KIEs is also important.) Furthermore, the low-frequency transitional modes are not expected to have significant effects in the tunneling contribution to the KIEs and SKIEs since they contribute very little either to the tunneling barrier or to the shortening of the tunneling paths. The anharmonicity could modify the variational effects and thus the variational contribution to the KIE and SKIE. However, as shown in Tables 3, 4, 6, 8, and 9, the variational effects are small (i.e., the reactions are dominated by the central barriers), and the variational contributions to KIEs and SKIEs are all very close to unity. It seems unlikely that the variational

(35) We have also performed similar vibrational analysis as reported in ref 8 in which we sorted all of the vibrational modes of the reactant and transition state into three categories: (i) the high-frequency modes, including all of the C−H and O−H stretching vibrations, (ii) the transitional modes, and (iii) medium-frequency modes, consisting of modes not included in (i) and (ii). The vibrational partition functions are calculated for every mode as functions of temperature. Then, according to the above grouping, the vibrational contributions to the KIEs and SKIEs as functions of temperature of each vibrational category are obtained. It is found that in the temperature range of 200−600 K, the high-frequency modes contribute most normally to the KIEs and most inversely to the SKIEs. Also, most of the temperature dependence of the vibrational contributions come from the high-frequency modes.

contributions would be modified significantly by anharmonicity in the current system except at very high temperatures. With the above assessment, we conclude that, while an accurate and totally consistent treatment of anharmonicity in the rate constant calculation is not currently available, the calculated KIEs and SKIEs in this study are at least semiquantitatively correct.

Summary

We have performed dual-level VTST with semiclassical tunneling calculations on the reaction rate constants with different barrier heights for the microsolvated E2 reactions of (1) $FO^-(H_2O) + C_2H_5Cl$, (2) $FO^-(H_2O) + C_2D_5Cl$, and (3) $FO^-(D_2O) + C_2H_5Cl$. The KIEs (ratios of the rate constants of the first and the second reactions) and the SKIEs (ratios of the rate constants of the first and the third reactions) have been obtained and factorized. As expected, when tunneling is not considered, the vibrational contribution is most responsible for the normal KIEs and inverse SKIEs. If tunneling is included in the calculation, we find that it contributes significantly to the calculated rate constants in most cases. Furthermore, tunneling plays an important role in determining both the KIEs and the SKIEs. The tunneling effects *lower* the normal E2 KIEs significantly at lower temperatures but may slightly increase the KIEs at high temperatures in high-barrier cases. It is also found that the tunneling effects increase the inverse SKIEs of the microsolvated E2 reaction. Our current study thus suggests that in E2 reactions, when tunneling is important, the observed normal KIEs at low temperatures may not be as pronounced as expected from the zero-point energy difference alone, and the SKIEs will also be less apparent (closer to one) compared to systems without tunneling.

Acknowledgment. This research project is supported in part by the National Science Council of Taiwan, Republic of China; Grant No. NSC 88-2113-M-194-008. We are also very grateful for the technical support by the National Center for High-Performance Computing (NCHC) in Hsing-Chu, Taiwan.

Supporting Information Available: Tables of absolute energies, optimized geometries, and vibrational frequencies for stationary points at various levels; Arrhenius plots of rate constants (PDF). This material is available free of charge via the Internet at http://pubs.acs.org.

JA991901E